https://ntrs.nasa.gov/search.jsp?R=20170005846 2019-05-01T04:35:40+00:00Z

This is an open access article published under an ACS AuthorChoice License, which permits copying and redistribution of the article or any adaptations for non-commercial purposes.

Environmental Science & Technology

Article

pubs.acs.org/est

Gridded National Inventory of U.S. Methane Emissions

Joannes D. Maasakkers,*[,†] Daniel J. Jacob,[†] Melissa P. Sulprizio,[†] Alexander J. Turner,[†] Melissa Weitz,[‡] Tom Wirth,[‡] Cate Hight,[‡] Mark DeFigueiredo,[‡] Mausami Desai,[‡] Rachel Schmeltz,[‡] Leif Hockstad,[‡] Anthony A. Bloom,[¶] Kevin W. Bowman,[¶] Seongeun Jeong,[§] and Marc L. Fischer[§]

[†]School of Engineering and Applied Sciences, Harvard University, Pierce Hall, 29 Oxford Street, Cambridge, Massachusetts 02138, United States

[‡]Climate Change Division, Environmental Protection Agency, Washington, District of Columbia 20460, United States

[¶]Jet Propulsion Laboratory, California Institute of Technology, Pasadena, California 91109, United States

[§]Energy Technologies Area, Lawrence Berkeley National Laboratory, Berkeley, California 94720, United States

ABSTRACT: We present a gridded inventory of US anthropogenic methane emissions with 0.1° × 0.1° spatial resolution, monthly temporal resolution, and detailed scale-dependent error characterization. The inventory is designed to be consistent with the 2016 US Environmental Protection Agency (EPA) Inventory of US Greenhouse Gas Emissions and Sinks (GHGI) for 2012. The EPA inventory is available only as national totals for different source types. We use a wide range of databases at the state, county, local, and point source level to disaggregate the inventory and allocate the spatial and temporal distribution of emissions for individual source types. Results show large differences with the EDGAR v4.2 global gridded inventory commonly used as a priori estimate in inversions of atmospheric methane observations. We derive grid-dependent error statistics for individual source types from comparison with the Environmental Defense Fund (EDF) regional inventory for Northeast Texas. These error statistics are independently verified by comparison with the California Greenhouse Gas Emissions Measurement (CALGEM) grid-resolved emission inventory. Our gridded, time-resolved inventory provides an improved basis for inversion of atmospheric methane observations to estimate US methane emissions and interpret the results in terms of the underlying processes.

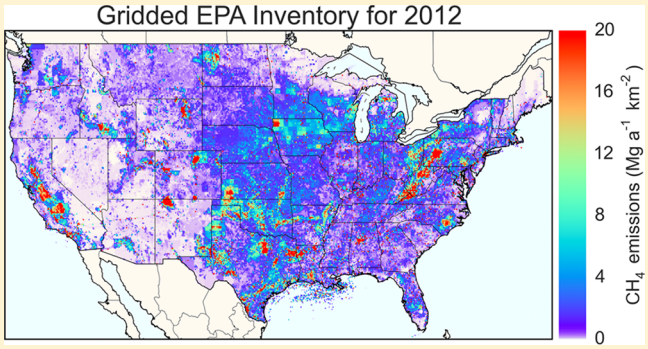

INTRODUCTION

Under the United Nations Framework Convention on Climate Change (UNFCCC), individual countries must report their national anthropogenic greenhouse gas emissions calculated using comparable methods.[1] The Intergovernmental Panel on Climate Change (IPCC)[2] provides three different methods or "tiers" for calculating emissions. All are bottom-up approaches in which emissions from individual source types are generally calculated as the product of activity data and emission factors. Increasing tiers are more detailed and require more country-specific data. In the United States, the Environmental Protection Agency (EPA) produces an annual Inventory of US Greenhouse Gas Emissions and Sinks (GHGI)[3] for reporting to the UNFCCC. The GHGI uses detailed information on activity data and emission factors, generally following IPCC Tier 2 and 3 methods. It provides detailed sectoral breakdown of emissions but only reports national totals for most source types. Here we present a spatially disaggregated version of the GHGI at 0.1° × 0.1° spatial resolution and monthly temporal resolution, including detailed information and error characterization for individual emission types. Our goal is to enable the use of the GHGI as an a priori estimate for inversions of atmospheric methane that may guide improvements in the inventory.

Table 1 gives the GHGI estimates for 2012 with methodology updated in 2016[3] and including contributions from different source types. Total US anthropogenic emission is 29.0 Tg a^{-1}, including major contributions from natural gas systems (24%), enteric fermentation (23%), landfills (20%), coal mining (9%), manure management (9%), and petroleum (or equivalently oil) systems (8%). The inventory includes forest fire emissions but no other natural sources. The main natural source of methane is thought to be wetlands, accounting for 8.5 ± 5 Tg A^{-1} in the contiguous US (CONUS).[4] Annual anthropogenic emissions from 1990 to 2014 computed by EPA[3] with a consistent method (revised each year to include updated information) show no significant trend and little interannual variability, with US totals staying in the range 28.6-31.2 Tg a^{-1} and contributions from individual source types varying by only a few percent.

Received: June 9, 2016
Revised: October 1, 2016
Accepted: October 13, 2016
Published: November 16, 2016

 © 2016 American Chemical Society

DOI: 10.1021/acs.est.6b02878
Environ. Sci. Technol. 2016, 50, 13123−13133

Table 1. Inventories of US Anthropogenic Methane Emissions (Gg a^{-1})[a]

source type	EPA GHGI (2012)	EDGAR v4.2 (2008)
agriculture		
enteric fermentation	6670 (5936−7871)	6720
manure management	2548 (2089−3058)	2200
rice cultivation	476 (395−557)	418
field burning of agricultural residues	11 (7−15)	38
natural gas systems	6906 (5594−8978)	4758
production	4442	
processing	890	
transmission and storage	1116	
distribution	457	
waste		
landfills	5691 (3528−9333)	5230
municipal	5098	
industrial	593	
wastewater treatment	601 (367−613)	887
domestic	368	
industrial	232	
composting	77 (39−116)	83
coal mines		
coal mining	2658 (2339−3057)	4140
underground	2159	
surface	499	
abandoned coal mines	249 (204−309)	
petroleum systems	2335 (1775−5814)	1032
other		
forest fires	443 (62−1214)	17
stationary combustion	265 (156−676)	424
mobile combustion	86 (76−101)	104
petrochemical production	3 (1−4)	24
ferroalloy production	1 (1−1)	1
total	29020 (26698−36565)	26075

[a]Column two shows the EPA inventory of US Greenhouse Gas Emissions and Sinks (GHGI) for 2012 as updated in 2016.[3] 95% confidence intervals are in parentheses as provided by EPA, sometimes only for broad source categories. Column three shows the US component of the global EDGAR v4.2 inventory for 2008.[7] The gridded version of the EPA GHGI developed in this work includes separate files for all entries in this table.

Application of atmospheric methane observations to estimate emissions usually involves inversion of an atmospheric transport model, with consideration of a priori information from an emission inventory to regularize the results and achieve a Bayesian optimal estimate of emissions.[5,6] The inversion optimizes emissions on a grid, and the inventory used as a priori information must be available on that grid. In the absence of a gridded version of the GHGI, previous inverse studies for the US have relied on the global EDGAR inventory[7] which provides annual emissions at 0.1° × 0.1° resolution. EDGAR uses IPCC Tier 1 methods with international data sets, and only includes a limited breakdown by source type. National totals in EDGAR are generally consistent with EPA, as shown in Table 1, but we will see that there are large errors in spatial allocation that affect inverse analyses and their interpretation. Our gridded version of the GHGI not only provides a better a priori estimate but also a better basis for interpreting inversion results and hence improving our understanding of the underlying processes.

METHODS

We disaggregate the 2012 national emissions reported by the 2016 version of the GHGI[3] into a gridded 0.1° × 0.1° monthly inventory. The gridded inventory is consistent with the EPA national emission totals for each source type (each entry in Table 1) and distributes these emissions based on information at the state, county, subcounty, and point source levels. In this manner, our inventory is a gridded representation of the national GHGI. Similar disaggregation has been done for national methane inventories in Switzerland,[8,9] Australia,[10] and the United Kingdom.[11] We limit our domain to the CONUS, which accounts for over 98% of total US emissions on the basis of our state-level estimates. We use the 2012 emissions from the 2014 EPA GHGI published in 2016, which includes detailed descriptions of the methods used to calculate the national emissions.[3] The 2014 GHGI includes updates to the petroleum and natural gas emissions to reflect new studies.[3,12] We focus on the year 2012 as the latest year for which all spatial activity data are available. Updating our gridded inventory to newer iterations (the GHGI is updated annually) and later years will be straightforward as new activity data are released.

We start from the most detailed spatial information directly available from the GHGI. This information varies by source type. Livestock emissions are available for each state, whereas waste and petroleum systems emissions are only available as national totals. Separate from the national inventory, EPA also collects methane emission and supporting data from large facilities under the Greenhouse Gas Reporting Program (GHGRP).[13] Facilities with emissions greater than 25 Gg CO_2 equivalent a^{-1} (corresponding to 0.11 tons h^{-1} for a pure methane source) and subject to the applicable regulatory requirements must report to the GHGRP. Some emissions reported to the GHGRP are directly measured (e.g., underground coal mines), while others are calculated on the basis of facility-level activity data (e.g., landfills). Where possible, we use facility-level emissions from the GHGRP but those sometimes need to be adjusted, as discussed below, to be consistent with the national inventory.

Agriculture. Emissions from agriculture include enteric fermentation, manure management, rice cultivation, and field burning of agricultural residues. EPA provides annual state-level enteric fermentation and manure management emissions for different animal types, taking into account varying practices across the country. We estimate county-level emissions by using livestock numbers for 14 different animal types (including different types of cattle) from the 2012 US Department of Agriculture Census of Agriculture for each animal type.[14] County-level emissions are allocated to the 0.1° × 0.1° grid using 9 different livestock occurrence probability maps (again distinguishing between different types of cattle) from USDA based on landtype.[15] Emissions from enteric fermentation are assumed to have no intra-annual variability. Emissions from manure management vary with temperature as given by[16]

$$f = \exp\left[\frac{A(T_m - T_o)}{RT_oT_m}\right] \quad (1)$$

where f is a monthly scaling factor, A = 64 kJ mol^{-1} is the activation energy, R is the ideal gas constant, T_m is the monthly average surface skin (radiant) temperature, and T_o = 303 K.[16]

DOI: 10.1021/acs.est.6b02878
Environ. Sci. Technol. 2016, 50, 13123−13133

Monthly emissions are calculated by scaling annual emissions with normalized monthly *f*-fields using 0.625° × 0.5° monthly average surface skin temperature fields from the NASA MERRA-2 meteorological data.[17] Livestock emissions also vary subanually as a function of varying herd size, and management practices but those effects are not included in our inventory.

Annual state-level emissions from rice cultivation are obtained from EPA and allocated to counties using acreage harvested from the USDA Census.[14] Emissions for each county are allocated to the 0.1° × 0.1° grid based on crop maps with 30 m resolution from the USDA Cropland Data Layer product.[18] Annual emissions are then distributed over individual months using normalized mean 2001−2010 heterotrophic respiration rates from the 1° × 1° monthly Carbon Data-Model Framework (CARDAMOM) terrestrial C cycle analysis.[19]

Emissions from field burning of agricultural residues of five individual crops (corn, rice, soybeans, sugar cane, and wheat) are allocated to a 2003−2007 monthly climatology of agricultural fires.[20]

Natural Gas Systems. This source type includes emissions from natural gas production, processing, transmission, and distribution. It does not include emissions from abandoned wells.[21] Emissions from natural gas production are available from EPA for each of the six National Energy Modeling System (NEMS) regions defined by the US Energy Information Administration (EIA).[22] The GHGI attributes emissions to different activities (e.g., vessel blowdowns, well workovers, liquid unloading) and equipment (e.g., pneumatic devices). Detailed maps of these activities and equipment are not available. Therefore, we rely on monthly well data obtained from DrillingInfo.[23] Separate DrillingInfo data are available for the number of gas producing wells, nonassociated gas wells (gas-to-oil ratio over 100 mcf gas per barrel), coalbed methane wells, and coalbed methane well water production. We also distinguish conventional and unconventional wells as some emissions are specific to hydraulic fracturing. A well is flagged as unconventional if the drilling direction is horizontal as given by DrillingInfo or if the reservoir type is coalbed, low permeability, or shale.[3] For each NEMS region, we allocate emissions using the DrillingInfo-based maps best representative of the spatial distribution of the considered activity or equipment. State-level condensate production from EIA[24] is combined with nonassociated gas well maps to allocate emissions from condensate tank vents. Three gas-producing states (Illinois, Indiana, and Tennessee) do not have active wells in the DrillingInfo database and amount to less than 1% of national active gas wells.[25] For these states we use state-level data on the number of natural gas wells[25] to calculate state emissions and then use county-level gas production[26] and finally three different well databases to grid emissions.[27−29] For offshore emissions, the 2011 Gulfwide Offshore Activity Data System (GOADS) platform-level emission database is used for the Gulf of Mexico[3,30] and DrillingInfo is used outside of the Gulf of Mexico, scaling total emissions to the national emission from the GHGI. As no national spatial data are available for gathering processes (only a subset report to the GHGRP[31]), emissions from these processes are included in the production sector and gridded in the same way.

Emissions from gas processing are only available as national totals in the GHGI. We allocate emissions to processing plants by combining the GHGRP data[13] with the EIA database for these plants.[32] The GHGRP covers 85% of the processed gas flow from the EIA database. For the remaining plants in the EIA database, emissions are estimated by multiplying their gas flow with the average ratio of methane emissions to gas flow of the GHGRP plants. Subsequently, emissions from all plants are scaled to match the national GHGI number; the scaling is required because the GHGRP does not include all emitting processes occurring at the plants and has different emission estimates per process.[31] Thus, we only use the GHGRP to allocate emissions in a relative sense with emission magnitudes constrained by the GHGI. The EIA database only provides postal codes for the processing plants and not coordinates; we determine non-GHGRP plant coordinates from the Rextag Strategies US Natural Gas Pipeline and Infrastructure Wall Map.[33] If there is no match with the GHGRP or Rextag data, emissions from the plant in the EIA database are spread out over the associated postal code area.[34]

EPA provides national emissions for different parts of the transmission sector. Most important are transmission compressor stations, for which we use a similar mapping as for processing plants. The GHGRP data for individual compressor stations are complemented with the EIA database for nonreporting compressor stations.[35] Emissions for nonreporting compressor stations are estimated based on their throughput,[35] using the average ratio of throughput to methane emission from the GHGRP data. Emissions are then scaled to the national total so our results are not affected by potential underestimates in the GHGRP emissions.[36] Similarly, a database of storage stations[37] is combined with the GHGRP using total field capacity to predict emissions. Locations are based on the GHGRP, supplemented by gas storage field locations georeferenced from the Rextag Strategies US Natural Gas Pipeline and Infrastructure Wall Map,[33] and DrillingInfo.[23] Similar approaches are also used for liquid natural gas (LNG) storage[38] and LNG import terminals.[39] Emissions from pipeline leaks and transmission meter and regulator stations are allocated to the network of interstate and intrastate pipelines.[40] Emissions from farm taps are allocated to pipelines intersecting with agricultural land.[18] Emissions related to storage at wells are mapped to all nonassociated gas wells.[23]

Emissions from different parts of the distribution network are available from EPA as national estimates. State-level emissions from distribution pipeline leaks are calculated using state data on pipeline miles and services from the Pipeline and Hazardous Materials Safety Administration (PHMSA) of which the sum is used for the national GHGI.[41] This takes into account different materials (e.g., cast iron, plastic) with different emission factors. Emissions from distribution meter and regulator stations are divided among states using state-level aggregated GHGRP information (no finer spatial information is available). Other distribution emissions are partitioned between the states based on leaked gas volume data from EIA.[42] Within states, emissions are mapped to 0.1° × 0.1° population data from the 2010 US Census.[43]

Waste. Waste emissions include landfills, wastewater treatment, and composting, for which EPA provides national totals following the categories in Table 1. We allocate emissions from landfills based on a combination of data from the GHGRP (1231 municipal landfills, 175 industrial landfills), the Landfill Methane Outreach Program (LMOP, municipal landfills only),[44] and the Facility Registration Service (FRS).[45] GHGRP landfills are assigned their reported emissions. 900 of 2049 LMOP landfills do not report emissions to the

DOI: 10.1021/acs.est.6b02878
Environ. Sci. Technol. 2016, 50, 13123−13133

GHGRP. For those we estimate emissions from GHGRP-reporting landfills with similar attributes (presence of a collection system, flares). Some landfills report landfill gas production through the LMOP. For the other landfills, waste in place is used as estimation metric combined with a decay factor for landfills that closed before 2012.[46] For landfills without any data (108), we assign the median emissions from the landfills for which information was available. Finally, we use landfills with known coordinates from the FRS that are not present in the GHGRP or LMOP data sets. We decide whether a landfill is municipal or industrial based on keyword descriptors in the databases. The 722 municipal FRS landfills are assigned the median emission derived from above, after which all non-GHGRP emissions are scaled to match the national emission estimate. For industrial landfills, the national estimate minus the GHGRP emissions is uniformly allocated across the 2309 industrial landfills from the FRS.

Emissions from wastewater treatment are reported as municipal or industrial in the GHGI. Facilities that report to the GHGRP account for 84% of the national industrial wastewater treatment emissions. To allocate the remaining industrial emissions as well as the municipal emissions, we use facility-level wastewater flow data from the Clean Watersheds Needs Survey.[47] Industrial wastewater treatment emissions are mapped to treated industrial flow, emissions from municipal septic systems to decentralized municipal flow, and centralized municipal systems emissions to centralized municipal flow.

State-level emissions from composting are calculated using the tonnage of municipal solid waste composted or, if composting data are not available, from the correlated tonnage recycled.[48] Within states, emissions are allocated to locations from the US Composting Council,[49] BioCycle composter database,[50] and composting entries in the FRS.[45] If there are fewer than three facilities found in a state, we allocate based on gridded population instead.[43]

Coal Mines. We allocate coal mining emissions using state-level emission estimates produced for the GHGI (M. Coté, Ruby Canyon Engineering, unpublished data) for underground mines and surface mines. These estimates account for methane recovered or destroyed, as well as postmining emissions (methane released during coal handling and processing). We use the locations and production of all active surface and underground coal mines from EIA.[51] A large number of underground mines report their annual methane emissions to GHGRP. We estimate emissions from nonreporting underground mines based on their share of the state total coal production combined with the state-level emissions, weighted by the basin-level in situ methane content of the coal for states that have mines in multiple basins.[3] Subsequently, we scale the emissions from nonreporting mines so that the total national emissions (including the GHGRP mines) match the GHGI. For surface mines, no GHGRP data are available. Emissions are allocated using the EPA state-level data as given above, combined with EPA basin-level emission factors and EIA mine-level production data. Similarly, postmining emissions are allocated to all mines based on their production and basin-specific emission factors.

The GHGI also includes emissions from abandoned coal mines. We start from the Abandoned Coal Mine Methane Opportunities Database (ACMMOD)[52] and add recently closed coal mines plus county-level estimates of mine closures before 1972 not included in ACMMOD (unpublished data produced for EPA by Ruby Canyon Engineering). For all closed mines, estimates of closure dates, status (venting, sealed, flooded), and estimates of emissions when the mine was active are available or estimated from county-level averages, allowing the estimation of present-day emissions based on decline equations used in the GHGI.[53] ACMMOD only includes mine locations on the county level. Precise locations of approximately one-third of the abandoned mines are found in the Full Mine Info data set.[54] The remaining emissions are allocated on the county level.

Petroleum Systems. The GHGI includes national emissions from different activities and equipment related to petroleum production, refining, and transport. We use monthly well data for several production quantities from DrillingInfo[23] to spatially allocate these emissions. These include total, heavy, and light oil production, with the cutoff between the last two at an American Petroleum Institute (API) gravity of 20. EPA estimates some emissions separately for heavy and light oil production. Furthermore, we created maps of oil wells (defined as wells with a produced gas-to-oil ratio under 100 mcf per barrel, wells with a higher ratio are classified as nonassociated gas wells), stripper wells (producing fewer than 10 barrels per day), and total and unconventional oil well completions. Similar to the allocation of natural gas production emissions, states without active wells in DrillingInfo are represented using state-specific data sets and amount to less than 1% of national production.[55] For the other states, the national-level emissions from each activity and device are allocated using the DrillingInfo maps. For example, emissions from well drilling are mapped to well completions, while emissions from heavy crude oil wellheads are mapped to heavy oil wells. As for natural gas systems, offshore emissions are based on the GOADS database for the Gulf of Mexico and DrillingInfo elsewhere. Emissions from petroleum refining are allocated to GHGRP facilities based on their reported emissions. National emissions from petroleum transportation are divided between the wells, offshore platforms, and refineries.

Other. Other refers to a number of smaller sources listed in Table 1. National forest fire emissions from the GHGI are distributed on a daily basis at $0.1° \times 0.1°$ resolution using the Quick Fire Emissions Data set (QFED v2.4) for 2012.[56] Stationary combustion emissions from electricity generation are calculated by multiplying plant-level heat inputs from the Acid Rain Program with fuel type specific emission factors.[57] Additional stationary combustion emissions from the industrial, commercial, and residential sectors are based on state-level consumption of different types of fuel (coal, fuel oil, natural gas, and wood) as reported by EIA.[58] Within states, residential and commercial emissions are allocated based on population while industrial emissions are allocated based on combustion emissions reported to the GHGRP. National on-road mobile combustion emissions for individual vehicle types in the GHGI are allocated spatially by first calculating state-level vehicle miles traveled (VMT) for six types of roads: urban and rural for each of primary, secondary, and other (minor) roads[59] and attributing those to individual vehicle types.[59] These state totals are then mapped to the different road networks taken from the National Transportation Atlas[60] and US Census products.[61] Combustion emissions from rail transport are allocated over the US railroad network.[61] Emissions from agricultural equipment are uniformly spread out across all agricultural land.[18] Emissions from mining-related vehicles are allocated to active mines.[54] Construction and "other" mobile combustion emissions are mapped based on population.

DOI: 10.1021/acs.est.6b02878
Environ. Sci. Technol. 2016, 50, 13123−13133

National emissions from ferroalloy production and from the petrochemical industry are divided over the facilities reporting to the GHGRP based on their total reported emissions.

RESULTS AND DISCUSSION

Figure 1 shows the distribution of annual emissions on the 0.1° × 0.1° grid for the six general emission categories of the

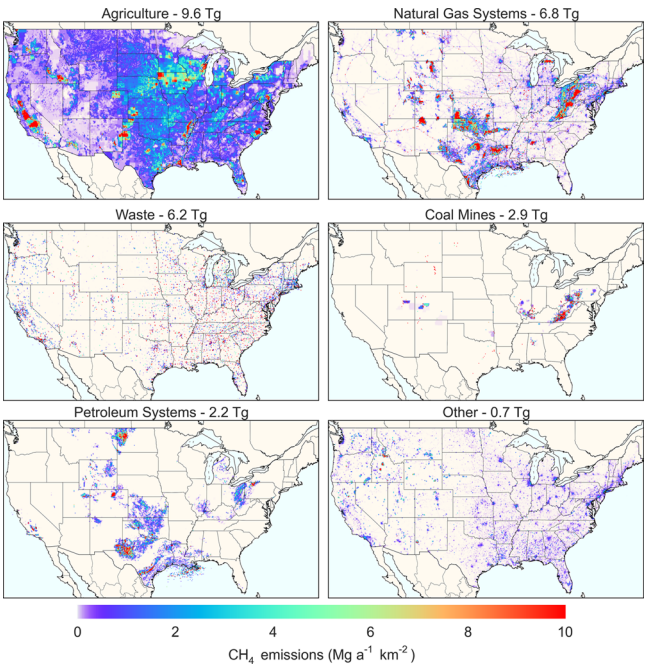

Figure 1. Contiguous US (CONUS) methane emissions from different source categories. Total annual US emissions from the 2016 EPA GHGI for 2012 are disaggregated here on a 0.1° × 0.1° grid. "Other" refers to the ensemble of minor sources in Table 1. (An equivalent figure for EDGAR v4.2 is shown by in Turner et al.[70]).

Methods section. Emissions from agriculture are broadly distributed across livestock farming areas. Hotspots are mostly from concentrated dairy cattle or hog populations such as in Iowa, North Carolina, and California. Rice cultivation contributes hotspots in northern California and along the lower Mississippi River. Emissions from natural gas systems are high in production fields, for example in Pennsylvania (Marcellus shale) and in Texas, with a maximum at Four Corners as found in top-down studies.[62] Waste emissions (dominated by landfills; Table 1) roughly map to population, with hotspots from large landfills and wastewater facilities. Coal mining emissions are concentrated in Appalachia. Petroleum systems emissions peak over the Bakken region in North Dakota and western Texas where natural gas emissions are low. Other emissions mostly feature forest fire hotspots in the West and stationary combustion emissions in populated areas.

Total CONUS emissions for 2012 are 28.7 Tg a^{-1}, slightly lower than the 29.0 Tg a^{-1} national total reported in Table 1 because of contributions from Alaska, Hawaii, and outside territories. Several sources vary monthly in our inventory including manure management, natural gas and petroleum production, stationary combustion, and forest fires (daily). Monthly emissions vary from 73 Gg per day in December to 89 Gg per day in July. Most of this monthly variation arises from manure management, which varies nationally from 2.4 Gg per day in January to 16.8 Gg per day in July. Eq 1 is for liquid storage systems but is applied here to all manure management systems, which may overestimate the seasonal variation.[63,64] For rice emissions, we assume a constant methane to CO_2 emission ratio from heterotrophic respiration, which may underestimate the seasonal variation as the ratio has been found to increase with temperature in wetlands and aquatic ecosystems.[65] On the other hand, some seasonal factors are not considered in our inventory due to lack of data such as livestock numbers, feed, and gas/petroleum distribution. Transient elevated emissions from oil/gas systems (the so-called "super-emitters"[66]) are also not resolved.

Figure 2 compares the distribution of total methane emissions in our gridded EPA inventory for 2012 to the EDGAR v4.2 inventory for 2008, the latest year of full release.[7] A fast track version of EDGAR (v4.2 FT2010[7]) has come out since but, based on visual inspection, the spatial emissions patterns in EDGAR v4.2 are of higher quality and most inverse studies have used EDGAR v4.2. There are large differences in spatial patterns between the Gridded EPA inventory and EDGAR v4.2, particularly for oil/gas systems and manure management. Emissions in the gridded EPA inventory are much higher over oil/gas production areas and lower over distribution (populated) areas. The two inventories show no significant correlation at their native 0.1° × 0.1° resolution (r = 0.06). The correlation increases to r = 0.42 at 0.5° × 0.5° resolution and r = 0.63 at 1.0° × 1.0° resolution.

Previous inverse studies for US methane emissions using EDGAR as a priori estimate have all found the need for a large upward correction of emissions in the South-Central US.[67−70] Figure 3 shows the distributions of livestock, oil/gas systems, and waste emissions for that region in the gridded EPA and EDGAR v4.2 inventories. The EDGAR v4.2 inventory places the oil/gas emissions in urban areas and completely misses areas of production. The oil/gas emissions in EDGAR v4.2 are strongly correlated with waste emissions because both are largely distributed following population. An inversion using EDGAR v4.2 as a priori estimate would not be able to separate the two and might wrongly attribute a source in oil/gas production regions to livestock. This stresses the importance of using a high-quality a priori inventory in inverse analyses, both to regularize the solution and to enable interpretation of results. Whereas different source types show spatial correlation in the EDGAR v4.2 inventory because of mapping to common databases, there is no such correlation between source types in our gridded EPA inventory even at 1° × 1° resolution. This separation between individual source types holds promise for interpreting results from inverse analyses.

Error characterization is necessary for a gridded emission inventory to serve as a priori estimate in Bayesian inversions and to interpret results from the inversions. Error characterization is not available for the EDGAR v4.2 inventory and inversions have typically assumed 30−100% uniform error based on expert judgment, or used the inversion to estimate the error in the a priori.[71] The GHGI includes detailed error characterization on its national totals for individual source types, based on propagation of uncertainties in the construction of the bottom-up estimates (Table 1). Errors in our 0.1° × 0.1° gridded inventory may be larger because of local uncertainties in activity data and emission factors, including the precise localization of emissions. For the same reason, averaging our inventory over coarser grids (by adding contributions from 0.1° × 0.1° grid cells) could reduce the error. This scale dependence is important to describe because inversions may seek to

DOI: 10.1021/acs.est.6b02878
Environ. Sci. Technol. 2016, 50, 13123−13133

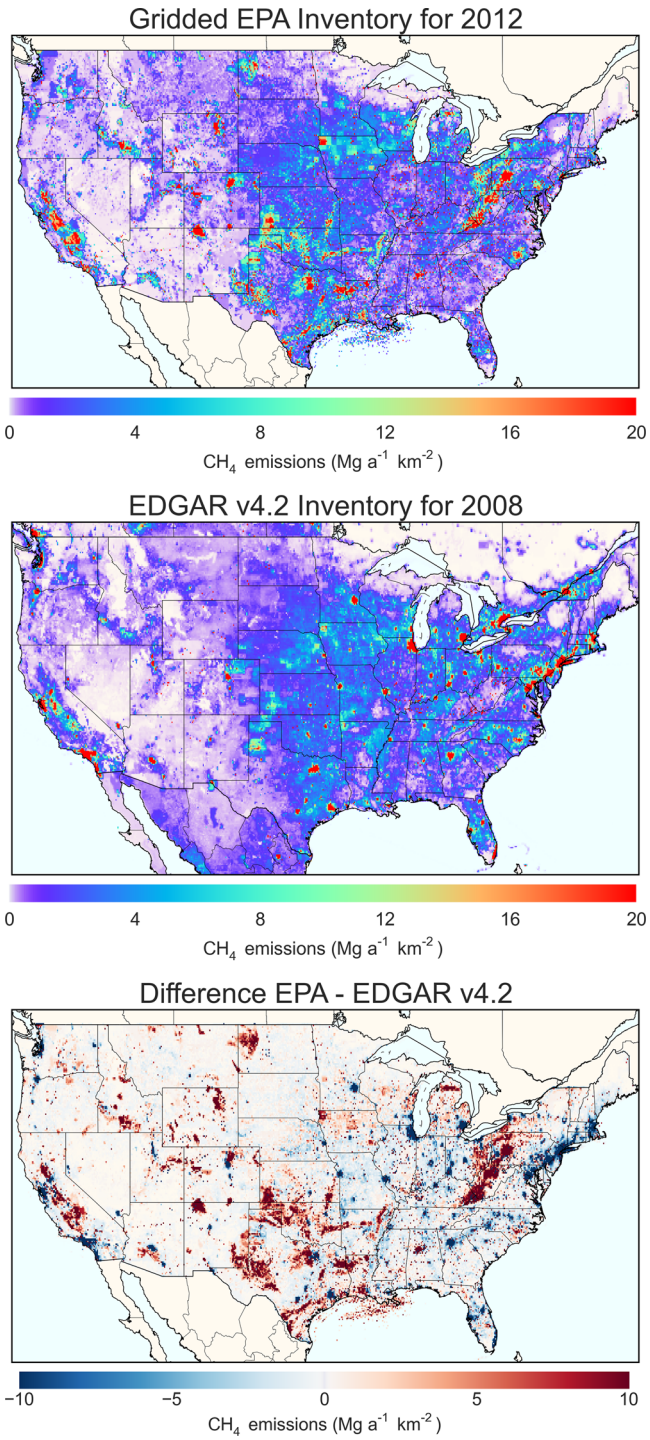

Figure 2. Total methane emissions in the gridded EPA inventory for 2012 (top), EDGAR v4.2 for 2008 (middle), and difference between the two (bottom).

optimize emissions at different spatial resolutions depending on the information content of the atmospheric observations.

Here we derive scale-dependent error statistics for our gridded EPA inventory by comparison to a detailed bottom-up emission inventory compiled by Environmental Defense Fund (EDF) for the ~300 × 300 km^2 Barnett Shale region in Northeast Texas by Lyon et al.[72] and subsequently updated with top-down constraints by Zavala-Araiza et al.[73] The EDF inventory was constructed largely independently from the GHGI. It is based on an extensive field campaign in the region in September−October 2013 including measurements of individual facilities as well as regional surveys.[12] The Barnett Shale region is of particular interest as a comparison standard because it includes diverse sources: the largest oil/gas field in the CONUS (30 000 active wells), major livestock operations, and the metropolitan area of Dallas/Fort Worth. The EDF inventory incorporates considerable local information that goes beyond the databases used in constructing our inventory, and including for example precise locations of dairy farms, gas gathering stations, and landfills.[72] Emissions are reported on a 4 × 4 km^2 grid (approximately 0.04° × 0.04°) with detailed breakdown by source types and statistical sampling of "super-emitter" facilities with anomalously large emissions.

Figure 4 shows emissions from livestock, natural gas, waste, and petroleum in the Zavala-Araiza EDF Barnett Shale inventory and compares to our gridded EPA inventory. Emission totals for the domain are shown in Table 2. There is a large difference in the magnitude of the source from oil/gas production, at least in part because Zavala-Araiza et al. find a larger frequency of superemitters than assumed in the GHGI emission factors. Despite this difference in magnitude there is a strong spatial correlation on the 0.1° × 0.1° grid (r = 0.78), implying that correction to the gridded EPA distribution in an inversion of atmospheric data could be reliably attributed to the oil/gas production source type, smoothing temporally over superemitters. The spatial correlation coefficient of the livestock source between the gridded EPA and EDF inventories is only 0.37 at 0.1° × 0.1° resolution but increases to 0.88 at 0.5° × 0.5° resolution. The gridded EPA inventory misses the exact locations of farms but this error is smoothed out on the county scale.

We take the Zavala-Araiza EDF Barnett Shale inventory as our best approximation of emissions in the region in order to derive scale-dependent error statistics for different source types that can be used in an inversion of atmospheric concentration data. We assume for this purpose that the total error probability density function (pdf) for each source type in a given grid cell is Gaussian and includes a displacement error due to imprecise localization. Our error model is given by

$$\sigma(\mathbf{x}) = \alpha\sqrt{\sum_{\mathbf{x}'} E(\mathbf{x}')^2 \exp\left(\frac{-\|\mathbf{x}-\mathbf{x}'\|^2}{\beta^2}\right)^2} \tag{2}$$

Here, $\sigma(\mathbf{x})$ is the Gaussian error standard deviation for the grid cell centered at location $\mathbf{x}$ and for a given source type, α is a base relative error standard deviation assuming no displacement error, $E(\mathbf{x}')$ is the 2-D field of emissions for that source type over all grid cells, and β is a length scale for the displacement error. α and β are assumed to be uniform for a given source type. We find optimal values for α and β by minimizing a least-squares cost function $J(\alpha, \beta)$ for the difference between our estimated error standard deviation and the absolute difference between the gridded EPA and EDF emissions:

$$J(\alpha, \beta) = \sum_{\mathbf{x}} (\sigma(\alpha, \beta, \mathbf{x}) - |E(\mathbf{x}) - E_{\mathrm{EDF}}(\mathbf{x})|)^2 \tag{3}$$

where the summation is over all grid cells of the Barnett Shale domain in Figure 4. Optimization of α and β is done for the different source types of Figure 4 (also separating waste as landfills and wastewater) and for grid resolutions L from 0.1° to 0.5° to determine the scale dependence of the error. 0.5° is the coarsest scale that can be usefully constrained from the Barnett Shale inventory, but from there we can extrapolate to the

DOI: 10.1021/acs.est.6b02878
Environ. Sci. Technol. 2016, 50, 13123−13133

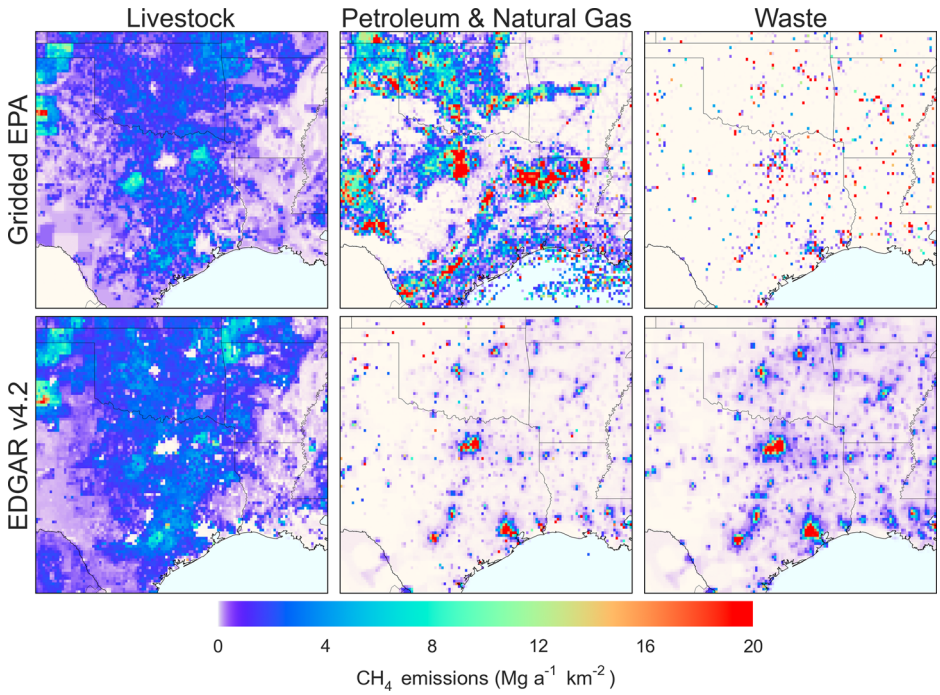

Figure 3. Emissions from livestock, oil/gas systems, and waste over the South-Central US in the gridded EPA inventory for 2012 and the EDGAR v4.2 inventory for 2008.

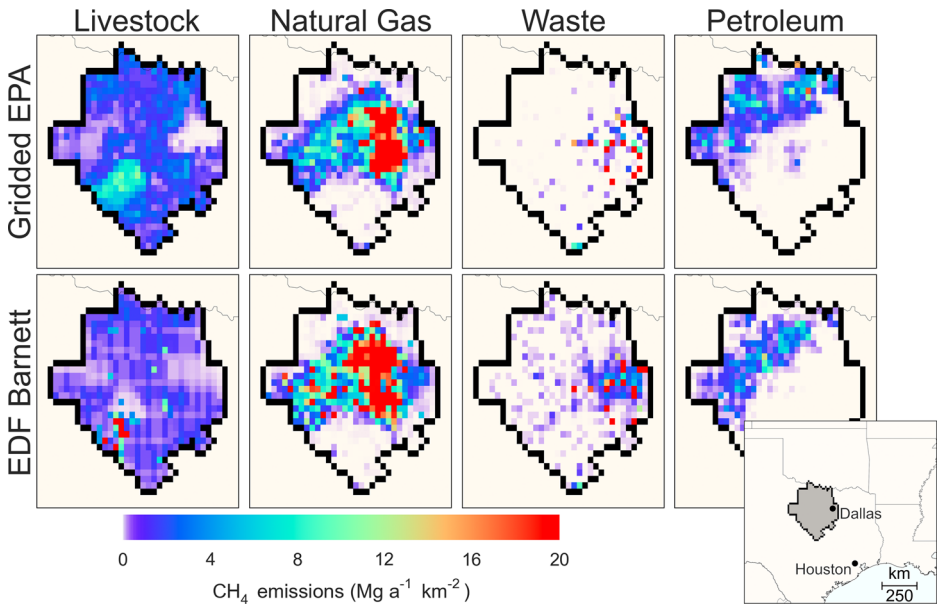

Figure 4. Methane emissions in the Barnett Shale region of Northeast Texas. Values for the four main categories are shown for our gridded EPA inventory and for the EDF inventory[73] at 0.1° × 0.1° resolution. The original EDF inventory is at 4 × 4 km^2 and is regridded here to 0.1° × 0.1° for comparison with our inventory. The location of the Barnett Shale region is shown inset. Emission totals for the region are given in Table 2.

national scale using the GHGI error estimates. For this purpose we take the average of the upper and lower confidence intervals for the given source type in Table 1 as representing the relative error standard deviation α_N on the national scale. We then fit our results for $\alpha(L)$ and $\beta(L)$ to exponential forms of L, with asymptote α_N for α. This yields

$$\alpha = \alpha_0 \exp(-k_\alpha(L - L_0)) + \alpha_N \quad (4)$$

$$\beta = \beta_0 \exp(-k_\beta(L - L_0)) \quad (5)$$

Here $L_0 = 0.1°$ is the native resolution of our inventory, and k_α and k_β (in units of inverse degrees) are smoothing coefficients that express the scale dependence of the error. The fit is subject to the condition $\alpha_0 \geq 0$; if the base error standard deviation derived from the Barnett Shale inventory is smaller than α_N then we assume that α is scale-independent and equal to α_N.

Figure 5 shows the base relative error standard deviation α and displacement length scale β as a function of grid resolution L for the different source types active in the Barnett Shale. Values for all coefficients in eqs 4 and 5 are given in Table 3. Base error standard deviations (α) for different source types at

DOI: 10.1021/acs.est.6b02878
Environ. Sci. Technol. 2016, 50, 13123−13133

Table 2. Regional Methane Emissions (Gg a^{-1})[a]

source	Barnett Shale region				California		
	EDF (Lyon)	EDF (Zavala-Araiza)	this work	r	CALGEM	this work	r
oil/gas production	330	436	327	0.78	171	264	0.90
gas processing	49	65	62	0.24	12	7	0.25
gas transmission	16	2	8	0.20	22	24	0.69
gas distribution	10	9	16	0.87	131	39	0.98
livestock	104	102	122	0.37	721	885	0.46
landfills	105	99	92	0.76	316	507	0.86
wastewater	7	7	12	0.21	91	45	0.53
sum	621	720	640	0.68	1463	1772	0.66

[a]Anthropogenic emissions from the Barnett Shale region in Northeast Texas (Figure 4) and from the state of California (Figure 6). Regional totals by source type from our gridded version of the gridded EPA inventory for 2012 (this work) are compared to the original bottom-up (Lyon) EDF inventory for the Barnett Shale in October 2013,[72] the updated (Zavala-Araiza) EDF inventory including top-down information,[73] and the CALGEM inventory for California in 2008 (livestock/waste)[63,74] and 2010 (oil/gas).[75] Also shown are spatial correlation coefficients r on the 0.1° × 0.1° grid for the Barnett Shale[73] and 0.2° × 0.2° for California.

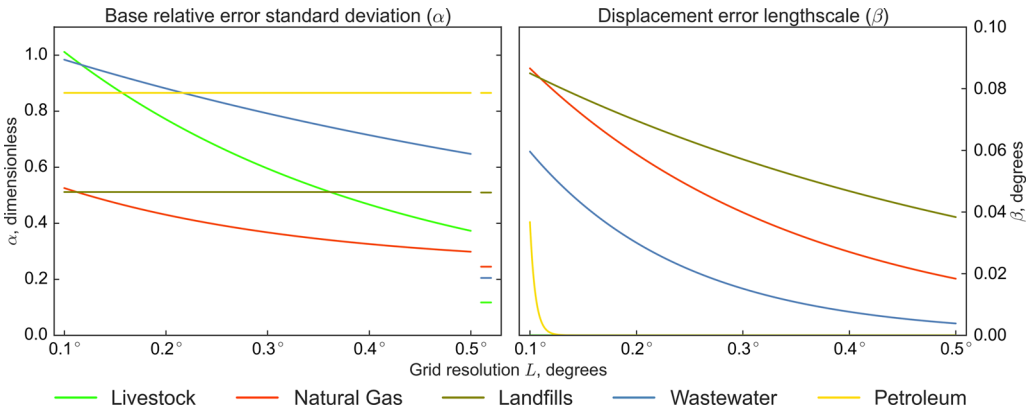

Figure 5. Relative error standard deviations for methane emissions from individual source types and their scale dependences. The figure shows the error parameters α and β used in eq 2 to calculate the absolute error standard deviations for a given $L \times L$ grid cell and source type as a function of the grid resolution L. The native grid resolution of the inventory is 0.1° × 0.1°, and averaging over coarser scales decreases errors for individual source types as described by exponential decay functions (eqs 4 and 5). The asymptotes for the base error standard deviations are the national values α_N shown as tick marks on the right side of the left panel. Values for all error parameters are given in Table 3.

Table 3. Error Parameters for the Gridded EPA Emission Inventory

source	α_0	k_α	α_N	β_0	k_β
livestock	0.89	3.1	0.12	0	
natural gas systems	0.28	4.2	0.25	0.09	3.9
landfills	0		0.51	0.08	2.0
wastewater treatment	0.78	1.4	0.21	0.06	6.9
petroleum systems	0		0.87	0.04	197

[a]Error parameters for use in eqs 4 and 5 to compute the base relative error standard deviation $\alpha(L)$ and displacement error length scale $\beta(L)$ for different source types at different grid resolutions $L \times L$. The resulting values of $\alpha(L)$ and $\beta(L)$ should be used in eq 2 to estimate the error standard deviation for a given source type and grid cell. Units are degrees for L and β_0, and inverse degrees for k_α and k_β. α_0 and α_N are dimensionless. The livestock error estimate is to be applied to the sum of enteric fermentation and manure management emissions.

0.1° × 0.1° grid resolution are all above 50%. Errors for livestock, natural gas systems, and wastewater are scale-dependent and decrease when coarser grid resolutions are used. Errors for petroleum systems and landfills are defined by the national estimates, which are relatively large, and are thus scale-independent. The displacement error measured by β is usually very small, less than 0.1°, in part because it is isotropic (there is no a priori information on the direction of displacement error). Because of its Gaussian form, it emphasizes the effect of neighboring misplacements; it would not capture the error from a distant misplacement or from a completely missing source.

We recommend that users of our emission inventory at a given grid resolution L apply the error parameters in Table 3 nationally to derive $\alpha(L)$ and $\beta(L)$ from eqs 4 and 5, and from there use eq 2 to derive the absolute error standard deviation σ for individual source types and grid cells. For source types not constrained by the Barnett Shale inventory, we assume here that the base error standard deviation at 0.1° × 0.1° resolution is 2.5 times the national value from Table 1, based on the median scale dependence for the sources in the Barnett Shale. We use median values of the other error parameters in Table 3 and cap α at 1.0. Error variances for the different source types present in a grid cell can be added in quadrature to derive the error variance for the total emission in that grid cell. A simple variogram analysis[76] of the difference between the EDF and EPA inventories shows no spatial error correlation, either for total emissions or for individual source types, suggesting that the a priori error covariance matrix needed for a Bayesian inversion can be assumed diagonal. A previous study comparing a disaggregated national inventory for Switzerland to EDGAR v4.2 did find significant spatial error correlations.[8]

DOI: 10.1021/acs.est.6b02878
Environ. Sci. Technol. 2016, 50, 13123−13133

Our error model is a first attempt to quantify grid-dependent errors for use in inversions of atmospheric concentration data, and in that it significantly improves on previous bottom-up inventories. It has however a number of weaknesses. First, the Barnett Shale region may not be representative nationally and offers no error characterization for some sources (in particular coal mining). Second, inverse analyses of atmospheric observations[67,70,77] suggest that EPA underestimates on the national scale maybe be larger than estimated from α_N, although these inverse analyses have their own errors. Third, the assumed Gaussian form for the error pdf is convenient for analytical inversions[6] but is not optimal. It does not exclude unphysical negative solutions and it does not capture the "fat tail" of the pdf contributed by superemitters.[66,72] A log-normal error pdf would solve the positivity problem and allow a better description of the fat tail. Fourth, some spatial error correlation would be expected even though it cannot be detected in our simple variogram analysis for the Barnett Shale; more advanced variogram analyses and better data sets might enable detection.[8,76] Fifth, we do not consider temporal error correlations because inversions typically focus on optimizing the spatial distribution while assuming the temporal variation to be known (and relatively weak in our case). This may not be appropriate for some applications, in particular when optimizing emissions from seasonally varying sources.[19]

The state of California has developed its own methane emission inventory in support of its policy objective to reduce greenhouse gas emissions to 1990 levels by 2020.[78] Similarly to our work here, this California inventory has been disaggregated by Zhao et al.,[74] Jeong et al.,[63] and Jeong et al.[75] to produce the gridded 0.1° × 0.1 ° California Greenhouse Gas Emissions Measurement (CALGEM) inventory (calgem.lbl.gov/emissions). The CALGEM grid is offset by 0.05° from ours, so we can only compare them at 0.2° × 0.2° and even then with some unresolvable remapping error. Table 2 compares total California emissions for individual source types, including spatial correlation coefficients. Total state emissions are close (1772 Gg a^{-1} in our work and 1463 Gg a^{-1} in CALGEM). There is more difference in individual source types but most source types show strong correlations between the two inventories, suggesting that they could be effectively constrained in an inverse analysis of atmospheric observations. Figure 6 compares the spatial distributions of emissions in the two inventories, including our (Barnett-based) estimated error standard deviation on the 0.2° × 0.2° grid, and adding error from different source types in quadrature for a given grid cell. We find that 51% of CALGEM emissions are from cells that have emission magnitudes within one standard deviation of our gridded EPA emissions. The largest differences are from livestock emissions, as CALGEM uses more local data to distribute these emissions within the large California counties.

In summary, we have constructed a gridded version of the EPA GHGI published in 2016 for US anthropogenic methane emissions with monthly 0.1° × 0.1° resolution including detailed information on different source types. Our inventory includes error characterization for different source types and spatial scales, as required for application as a priori estimate in inverse analyses. Our inventory is for 2012 emissions but can easily be updated to later years as activity data become available. Monthly gridded emission fields for all emission subcategories in Table 1 are publicly available at www.epa.gov/ghgemissions/gridded-2012-methane-emissions.

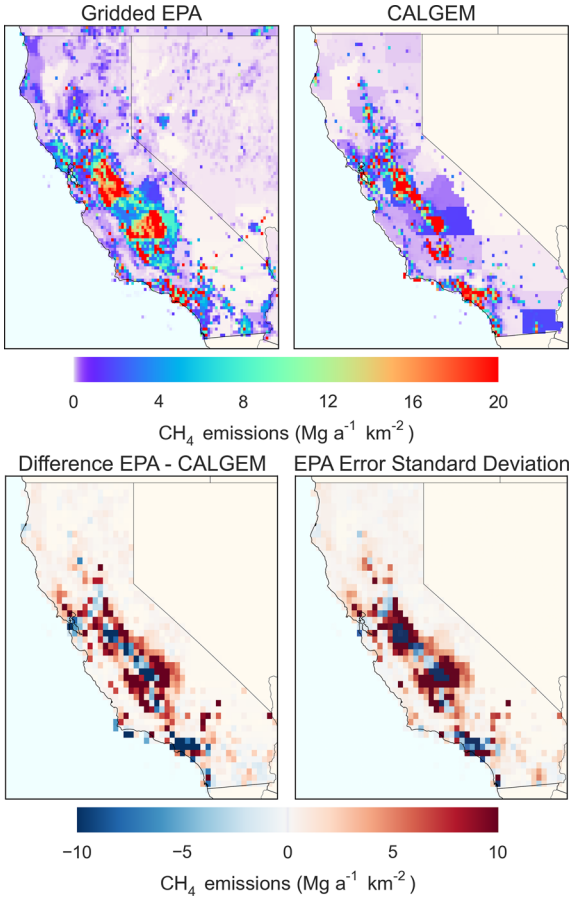

Figure 6. Methane emissions in California in 2012 from all sources in Table 2. The top panels show results from our gridded EPA inventory and from the CALGEM inventory on their native 0.1° × 0.1° grids. The bottom left panel shows the difference and the bottom right panel shows the error standard deviation in our gridded EPA inventory as computed with the method described in the text. The sign of the error standard deviation in the figure is the same as the EPA-CALGEM difference to facilitate visual comparison. Differences and error standard deviations are shown on a 0.2° × 0.2° grid to account for the 0.05° offset between the EPA and CALGEM grids.

AUTHOR INFORMATION

Corresponding Author

*E-mail: Maasakkers@fas.harvard.edu.

Notes

The authors declare no competing financial interest.

ACKNOWLEDGMENTS

This research was funded by the NASA Carbon Monitoring System (CMS). A.J. Turner was supported by a Department of Energy (DOE) Computational Science Graduate Fellowship (CSGF). Part of this research was carried out at the Jet Propulsion Laboratory, California Institute of Technology under a contract with NASA. Work by M.L. Fischer and S. Jeong at LBNL was supported by the NASA CMS program (NNH13ZDA001N) and the California Energy Commission Natural Gas Research Program under U.S. Department of Energy Contract No. DE-AC02-05CH11231. We thank D.R. Lyon, D. Zavala-Araiza, and S.P. Hamburg for providing the EDF methane emissions over the Barnett Shale. We thank the anonymous reviewers for their thorough comments.

DOI: 10.1021/acs.est.6b02878
Environ. Sci. Technol. 2016, 50, 13123−13133

REFERENCES

(1) United Nations. United Nations Framework Convention on Climate Change, Article 4(1)(a), , 1992. unfccc.int.

(2) IPCC. *Guidelines for National Greenhouse Gas Inventories*; Eggleston, H. S., Buendia, L., Miwa, K., Ngara, T., Tanabe, K., Eds.; The National Greenhouse Gas Inventories Programme: Hayama, Kanagawa, Japan, 2006.

(3) EPA. Inventory of US Greenhouse Gas Emissions and Sinks: 1990−2014, 2016. https://www.epa.gov/ghgemissions/us-greenhouse-gas-inventory-report-1990-2014.

(4) Melton, J.; Wania, R.; Hodson, E.; Poulter, B.; Ringeval, B.; Spahni, R.; Bohn, T.; Avis, C.; Beerling, D.; Chen, G.; et al. Present state of global wetland extent and wetland methane modelling: conclusions from a model intercomparison project (WETCHIMP). *Biogeosciences* **2013**, *10*, 753−788.

(5) Streets, D. G.; Canty, T.; Carmichael, G. R.; de Foy, B.; Dickerson, R. R.; Duncan, B. N.; Edwards, D. P.; Haynes, J. A.; Henze, D. K.; Houyoux, M. R.; et al. Emissions estimation from satellite retrievals: A review of current capability. *Atmos. Environ.* **2013**, *77*, 1011−1042.

(6) Jacob, D. J.; Turner, A. J.; Maasakkers, J. D.; Sheng, J.; Sun, K.; Liu, X.; Chance, K.; Aben, I.; McKeever, J.; Frankenberg, C. Satellite observations of atmospheric methane and their value for quantifying methane emissions. *Atmos. Chem. Phys. Discuss.* **2016**, *2016*, 1−41.

(7) European Commission. *Emission Database for Global AtmosphericResearch (EDGAR)*, 527 release version 4.2.; European Commission, 2011.

(8) Hiller, R.; Bretscher, D.; DelSontro, T.; Diem, T.; Eugster, W.; Henneberger, R.; Hobi, S.; Hodson, E.; Imer, D.; Kreuzer, M.; et al. Anthropogenic and natural methane fluxes in Switzerland synthesized within a spatially explicit inventory. *Biogeosciences* **2014**, *11*, 1941−1959.

(9) Henne, S.; Brunner, D.; Oney, B.; Leuenberger, M.; Eugster, W.; Bamberger, I.; Meinhardt, F.; Steinbacher, M.; Emmenegger, L. Validation of the Swiss methane emission inventory by atmospheric observations and inverse modelling. *Atmos. Chem. Phys.* **2016**, *16*, 3683−3710.

(10) Wang, Y.-P.; Bentley, S. Development of a spatially explicit inventory of methane emissions from Australia and its verification using atmospheric concentration data. *Atmos. Environ.* **2002**, *36*, 4965−4975.

(11) Defra. National Atmospheric Emissions Inventory, 2014. naei.defra.gov.uk.

(12) Harriss, R.; Alvarez, R. A.; Lyon, D.; Zavala-Araiza, D.; Nelson, D.; Hamburg, S. P. Using multi-scale measurements to improve methane emission estimates from oil and gas operations in the Barnett Shale region, Texas. *Environ. Sci. Technol.* **2015**, *49*, 7524−7526.

(13) EPA. Greenhouse Gas Reporting Program, 2013. epa.gov/ghgreporting/.

(14) USDA. *Census of Agriculture*; USDA-NASS: Washington, DC, 2012; quickstats.nass.usda.gov.

(15) USDA. *Census of Agriculture: Weighted Land Use/Cover Filter Files*; USDA-NASS: Washington, DC, 2012; agcensus.usda.gov/Publications/2012/Online_Resources/Ag_%20551%20Atlas_Maps/.

(16) Mangino, J.; Bartram, D.; Brazy, A. Development of a methane conversion factor to estimate emissions from animal waste lagoons. Presented at the US EPA 17th Emission 554 Inventory Conference, Atlanta, GA, April 2002.

(17) Bosilovich, M. G.; Lucchesi, R.; Suarez, M. File Specification for MERRA-2. GMAO Office Note No. 9 (Version 1.1), 2016. gmao.gsfc.nasa.gov/pubs/docs/Bosilovich785.pdf.

(18) USDA. *Cropland Data Layer*; USDA-NASS: Washington, DC, 2014; nassgeodata.gmu.edu/CropScape/.

(19) Bloom, A. A.; Exbrayat, J.-F.; van der Velde, I. R.; Feng, L.; Williams, M. The decadal state of the terrestrial carbon cycle: Global retrievals of terrestrial carbon allocation, pools, and residence times. *Proc. Natl. Acad. Sci. U. S. A.* **2016**, *113*, 1285−1290.

(20) McCarty, J. L. Remote sensing-based estimates of annual and seasonal emissions from crop residue burning in the contiguous United States. *J. Air Waste Manage. Assoc.* **2011**, *61*, 22−34.

(21) Kang, M.; Kanno, C. M.; Reid, M. C.; Zhang, X.; Mauzerall, D. L.; Celia, M. A.; Chen, Y.; Onstott, T. C. Direct measurements of methane emissions from abandoned oil and gas wells in Pennsylvania. *Proc. Natl. Acad. Sci. U. S. A.* **2014**, *111*, 18173−18177.

(22) DOE/EIA, NEMS—National Energy Modeling System: An Overview, 2009. http://www.eia.gov/forecasts/aeo/nems/overview/index.html.

(23) DrillingInfo, DI Desktop, 2015. didesktop.com.

(24) EIA. Annual Lease Condensate Production, 2012. eia.gov/dnav/ng/ng_prod_lc_s1_a.htm.

(25) EIA. Number of Producing GasWells, 2012. eia.gov/dnav/ng/ng_prod_wells_s1_a.htm.

(26) USDA. County-level Oil and Gas Production in the US, 2014. ers.usda.gov/data-products/county-level-oil-and-gas-production-in-the-us.aspx.

(27) Tennessee Department of Environment and Conservation. Oil and gas well permit data, 2015. http://environment-online.state.tn.us:8080/pls/enf_reports/f?p=9034:34300:::NO:::.

(28) Indiana Department of Natural Resources. Oil & Gas Online Well Records Database, 2015. in.gov/dnr/dnroil/5447.htm.

(29) Illinois State Geological Survey. ISGS Wells and Borings Database, 2015. clearinghouse.isgs.illinois.edu/data/geology/location-points-isgs-wells-and-borings-database.

(30) US Bureau of Ocean Energy Management. 2011 Gulfwide Emission Inventory, 2011. boem.gov/2011-Gulfwide-Emission-Inventory/.

(31) Marchese, A. J.; Vaughn, T. L.; Zimmerle, D. J.; Martinez, D. M.; Williams, L. L.; Robinson, A. L.; Mitchell, A. L.; Subramanian, R.; Tkacik, D. S.; Roscioli, J. R.; et al. Methane emissions from United States natural gas gathering and processing. *Environ. Sci. Technol.* **2015**, *49*, 10718.

(32) EIA. EIA-757 Natural Gas Processing Plant Survey, 2013. eia.gov/cfapps/ngqs/ngqs.cfm.

(33) *Natural Gas Pipeline and Infrastructure Wall Map*; Rextag Strategies, 2008.

(34) US Census Bureau. Cartographic Boundary Shapefiles: ZIP Code Tabulation Areas, 2013. census.gov/geo/maps-data/data/cbf/cbf_zcta.html.

(35) EIA, Office of Oil and Gas. The Crucial Link Between Natural Gas Production and Its Transportation to Market, 2006. http://www.eia.gov/pub/oil_gas/natural_gas/feature_articles/2006/ngprocess/ngprocess.pdf.

(36) Zimmerle, D. J.; Williams, L. L.; Vaughn, T. L.; Quinn, C.; Subramanian, R.; Duggan, G. P.; Willson, B.; Opsomer, J. D.; Marchese, A. J.; Martinez, D. M.; Robinson, A. L. Methane Emissions from the Natural Gas Transmission and Storage System in the United States. *Environ. Sci. Technol.* **2015**, *49*, 9374−9383.

(37) EIA. Natural Gas Underground Storage Facilities. EIA-191, Monthly Underground Gas Storage Report, 2014. eia.gov/maps/map_data/NaturalGas_UndergroundStorage_US_EIA.zip.

(38) EIA. LNG Peaking Shaving and Import Facilities, 2008. eia.gov/pub/oil_gas/natural_gas/analysis_publications/ngpipeline/lngpeakshaving_map.html.

(39) EIA; Federal Energy Regulatory Commission; US Dept. of Transportation. Liquefied Natural Gas Import/Export Terminals, 2013. eia.gov/maps/map_data/Lng_ImportExportTerminals_US_EIA.zip.

(40) EIA Natural Gas Interstate and Intrastate Pipelines. Collected by EIA from FERC and other external sources, 2012. eia.gov/maps/map_data/NaturalGas_InterIntrastate_Pipelines_US_EIA.zip.

(41) PHMSA, Office of Pipeline Safety. Gas Distribution Annual Data, 2012. phmsa.dot.gov/pipeline/library/data-stats.

(42) EIA, EIA-176 Natural Gas Deliveries. Available at: eia.gov/cfapps/ngqs/ngqs.cfm, 2013.

DOI: 10.1021/acs.est.6b02878
Environ. Sci. Technol. 2016, 50, 13123−13133

(43) US Census Bureau. US Census TIGER/Line Population and Housing Unit Counts, 2010. census.gov/geo/maps-data/data/tiger-data.html.
(44) EPA. Landfill Methane Outreach Program: Landfill-level data, 2015. epa.gov/lmop/projects-candidates/index.html#map-area.
(45) EPA. Facility Registry Service, 2015. epa.gov/enviro/geospatial-data-download-service.
(46) RTI International. *Solid Waste Emissions Inventory Support*, Review Draft; EPA, 2004.
(47) EPA. Clean Watersheds Needs Survey, 2008. epa.gov/cwns.
(48) Shin, D. Generation and Disposition of Municipal Solid Waste (MSW) in the United States: A National Survey. Master of Science Thesis, Columbia University, New York, 2014; http://www.seas.columbia.edu/earth/wtert/sofos/Dolly_Shin_Thesis.pdf.
(49) US Composting Council. Compost Locator Map, 2015. compostingcouncil.org/wp/compostmap.php.
(50) BioCycle. Find A Composter database, 2015. findacomposter.com.
(51) EIA. Coal Production and Preparation Report. Review Draft, 2013. eia.gov/maps/layer_info-m.cfm.
(52) EPA. Abandoned Coal Mine Methane Opportunities Database, 2008. https://www.epa.gov/sites/production/files/2016-03/documents/amm_opportunities_database.pdf.
(53) EPA. Methane Emissions from Abandoned Coal Mines in the US: Emission Inventory Methodology and 1990−2002 Emissions Estimates, 2004. https://nepis.epa.gov/Exe/ZyPDF.cgi/600004JM.PDF?Dockey=600004JM.PDF. Addendum to Methane Emissions from Abandoned Coal Mines in the US: Emission Inventory Methodology and 1990−2002 Emissions Estimates, 2007. https://www.epa.gov/sites/production/files/2016-03/documents/abandoned_mine_variables_by_basin.pdf.
(54) US Department of Labor Mine Safety and Health Administration. Full Mine Info dataset, 2015. http://developer.dol.gov/health-and-safety/full-mine-info-mines.
(55) EIA. Crude Oil Production, 2004. eia.gov/dnav/pet/pet_crd_crpdn_adc_mbbl_m.htm.
(56) Darmenov, A.; da Silva, A. The quick fire emissions dataset (QFED)-documentation of versions 2.1, 2.2 and 2.4. *NASA Technical Report Series on Global Modeling and Data Assimilation, NASA TM-2013−104606* **2013**, *32*, 183.
(57) EPA. Air Markets Program Data, 2012. ampd.epa.gov/ampd/.
(58) EIA. State Energy Data System, 2012. eia.gov/state/seds/.
(59) Federal Highway Administration. Highway Policy Information: Highway Statistics 2013. https://www.fhwa.dot.gov/policyinformation/statistics/2013/.
(60) US Department of Transportation. National Transportation Atlas Database, 2015. http://www.rita.dot.gov/bts/sites/rita.dot.gov.bts/files/publications/national_transportation_atlas_database/2015/index.html.
(61) US Census Bureau. TIGER/Line Shapefiles, 2012. census.gov/geo/maps-data/data/tiger-line.html.
(62) Kort, E. A.; Frankenberg, C.; Costigan, K. R.; Lindenmaier, R.; Dubey, M. K.; Wunch, D. Four corners: The largest US methane anomaly viewed from space. *Geophys. Res. Lett.* **2014**, *41*, 6898−6903.
(63) Jeong, S.; Zhao, C.; Andrews, A. E.; Sweeney, C.; Bianco, L.; Wilczak, J. M.; Fischer, M. L. Seasonal variations in CH_4 emissions from central California. *Geophys. Res. Lett.* **2012**, *117*, D11306.
(64) Owen, J. J.; Silver, W. L. Greenhouse gas emissions from dairy manure management: a review of field-based studies. *Glob. Change Biol.* **2015**, *21*, 550−565.
(65) Yvon-Durocher, G.; Allen, A. P.; Bastviken, D.; Conrad, R.; Gudasz, C.; St-Pierre, A.; Thanh-Duc, N.; Del Giorgio, P. A. Methane fluxes show consistent temperature dependence across microbial to ecosystem scales. *Nature* **2014**, *507*, 488−491.
(66) Zavala-Araiza, D.; Lyon, D.; Alvarez, R. A.; Palacios, V.; Harriss, R.; Lan, X.; Talbot, R.; Hamburg, S. P. Toward a Functional Definition of Methane Super-Emitters: Application to Natural Gas Production Sites. *Environ. Sci. Technol.* **2015**, *49*, 8167−8174. PMID: 26148555.
(67) Miller, S. M.; Wofsy, S. C.; Michalak, A. M.; Kort, E. A.; Andrews, A. E.; Biraud, S. C.; Dlugokencky, E. J.; Eluszkiewicz, J.; Fischer, M. L.; Janssens-Maenhout, G.; Miller, B. R.; Miller, J. B.; Montzka, S. A.; Nehrkorn, T.; Sweeney, C. Anthropogenic emissions of methane in the United States. *Proc. Natl. Acad. Sci. U. S. A.* **2013**, *110*, 20018−20022.
(68) Wecht, K. J.; Jacob, D. J.; Frankenberg, C.; Jiang, Z.; Blake, D. R. Mapping of North American methane emissions with high spatial resolution by inversion of SCIAMACHY satellite data. *J. Geophys. Res-Atmos.* **2014**, *119*, 7741−7756.
(69) Alexe, M.; Bergamaschi, P.; Segers, A.; Detmers, R.; Butz, A.; Hasekamp, O.; Guerlet, S.; Parker, R.; Boesch, H.; Frankenberg, C.; et al. Inverse modelling of CH 4 emissions for 2010−2011 using different satellite retrieval products from GOSAT and SCIAMACHY. *Atmos. Chem. Phys.* **2015**, *15*, 113−133.
(70) Turner, A. J.; Jacob, D. J.; Wecht, K. J.; Maasakkers, J. D.; Lundgren, E.; Andrews, A. E.; Biraud, S. C.; Boesch, H.; Bowman, K. W.; Deutscher, N. M.; Dubey, M. K.; Griffith, D. W. T.; Hase, F.; Kuze, A.; Notholt, J.; Ohyama, H.; Parker, R.; Payne, V. H.; Sussmann, R.; Sweeney, C.; Velazco, V. A.; Warneke, T.; Wennberg, P. O.; Wunch, D. Estimating global and North American methane emissions with high spatial resolution using GOSAT satellite data. *Atmos. Chem. Phys.* **2015**, *15*, 7049−7069.
(71) Ganesan, A.; Rigby, M.; Zammit-Mangion, A.; Manning, A.; Prinn, R.; Fraser, P.; Harth, C.; Kim, K.-R.; Krummel, P.; Li, S.; et al. Characterization of uncertainties in atmospheric trace gas inversions using hierarchical Bayesian methods. *Atmos. Chem. Phys.* **2014**, *14*, 3855−3864.
(72) Lyon, D. R.; Zavala-Araiza, D.; Alvarez, R. A.; Harriss, R.; Palacios, V.; Lan, X.; Talbot, R.; Lavoie, T.; Shepson, P.; Yacovitch, T. I.; et al. Constructing a spatially resolved methane emission inventory for the Barnett Shale Region. *Environ. Sci. Technol.* **2015**, *49*, 8147−8157.
(73) Zavala-Araiza, D.; Lyon, D. R.; Alvarez, R. A.; Davis, K. J.; Harriss, R.; Herndon, S. C.; Karion, A.; Kort, E. A.; Lamb, B. K.; Lan, X.; et al. Reconciling divergent estimates of oil and gas methane emissions. *Proc. Natl. Acad. Sci. U. S. A.* **2015**, *112*, 15597−15602.
(74) Zhao, C.; Andrews, A. E.; Bianco, L.; Eluszkiewicz, J.; Hirsch, A.; MacDonald, C.; Nehrkorn, T.; Fischer, M. L. Atmospheric inverse estimates of methane emissions from Central California. *J. Geophys. Res.* **2009**, *114*, D16302.
(75) Jeong, S.; Millstein, D.; Fischer, M. L. Spatially Explicit Methane Emissions from Petroleum Production and the Natural Gas System in California. *Environ. Sci. Technol.* **2014**, *48*, 5982−5990.
(76) Kitanidis, P. *Introduction to Geostatistics: Applications in Hydrogeology*; Cambridge University Press, 1997.
(77) Brandt, A.; Heath, G.; Kort, E.; O'sullivan, F.; Pétron, G.; Jordaan, S.; Tans, P.; Wilcox, J.; Gopstein, A.; Arent, D.; et al. Methane leaks from North American natural gas systems. *Science* **2014**, *343*, 733−735.
(78) California Air Resources Board. First Update to the Climate Change Scoping Plan, 2014. arb.ca.gov/cc/scopingplan/2013_update/first_update_climate_change_scoping_plan.pdf.

DOI: 10.1021/acs.est.6b02878
Environ. Sci. Technol. 2016, 50, 13123−13133